Nanoscale

www.rsc.org/nanoscale

Volume 5 | Number 10 | 21 May 2013 | Pages 3995–4518

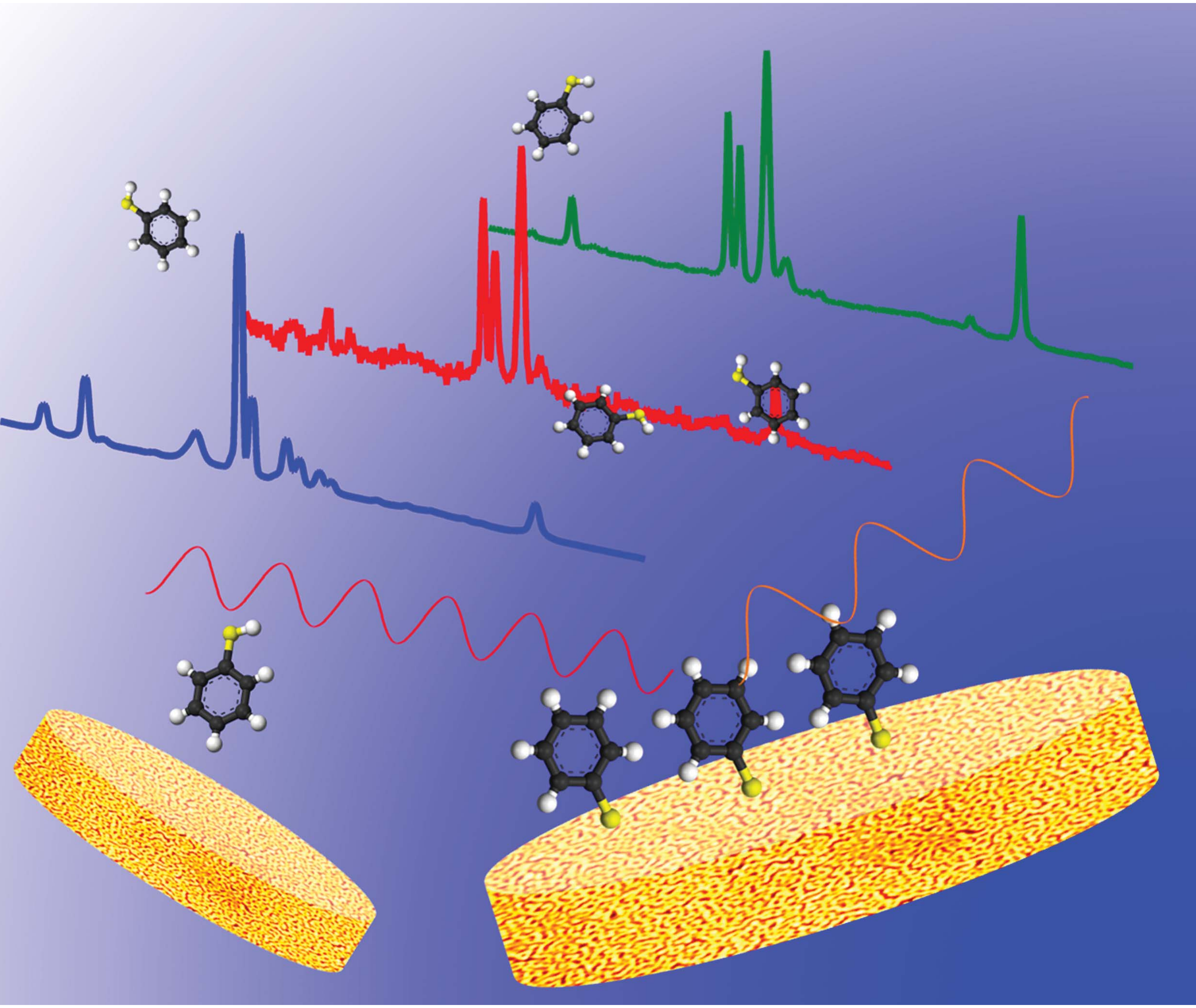

ISSN 2040-3364

RSC Publishing

COMMUNICATION
Shih *et al.*
Surface-enhanced Raman spectroscopy with monolithic nanoporous gold disk substrates

NCNST

Nanoscale

RSCPublishing

COMMUNICATION

Surface-enhanced Raman spectroscopy with monolithic nanoporous gold disk substrates†

Cite this: *Nanoscale*, 2013, **5**, 4105

Received 18th October 2012
Accepted 20th December 2012

DOI: 10.1039/c2nr33242f

www.rsc.org/nanoscale

Ji Qi, Pratik Motwani, Mufaddal Gheewala, Christopher Brennan, John C. Wolfe and Wei-Chuan Shih*

Monolithic hierarchical nanoporous gold disks, 500 nm in diameter, 75 nm in thickness and 3.5 nm in pore radius, have been fabricated by hybrid processes. A surface-enhanced Raman scattering enhancement factor of at least 10^8 has been obtained on individual disks using benzenethiol self-assembled monolayer with 785 nm laser excitation.

Surface-enhanced Raman scattering (SERS) has been widely applied to molecular detection and identification.[1–3] The technique derives its sensitivity from electrical field amplification by localized surface plasmon resonance (LSPR), strongest at SERS hot-spots associated with nanoscale gaps, and protrusions.[4] These observations have sparked intense interest in nanoporous gold (NPG) as SERS substrates, where porosities and pore diameters in ranges of 35–50% and 5–10 nm, respectively, have been reported.[5–8] An additional potential benefit is that internally adsorbed molecules and those that may be traversing the nanoporous network can also participate in Raman scattering.[4] Another potential advantage of NPG over non-monolithic SERS substrates, such as immobilized or aggregated nanoparticles, is the simplicity by which it can be integrated with sensor chip technology. It has been shown that the LSPR peak of NPG thin films exhibits a pore-size dependent redshift.[9,10] Although SERS activity has been documented, wide variations in SERS enhancement factors (EFs) have been reported;[6–8] possibly reflecting differences in material composition and morphology, fabrication technique, SERS marker, and/or excitation wavelength. Several groups have explored the increase in EF due to further processing of the NPG films; Zhang *et al.* observed a ~100-fold increase in EF caused by wrinkling the substrate of an NPG film, an approach that suffers from very wide site-to-site EF variation.[11] Jiao *et al.* also achieved a ~100-fold EF increase in mechanically stamped NPG gratings, which they attributed to the combined effect of improved light-coupling by the grating structure and mechanical densification.[12] Wi *et al.* reported a 5-fold increase in the SERS signal from NPG disk substrates compared to solid gold disks,[13] which are known to produce a SERS EF of 1000–10 000.[14,15] In their work, NPGDs were formed by dealloying co-sputtered gold and copper targets and patterned using electron-beam lithography. The disks were ~200 nm in diameter and 80 nm in thickness.

In this article, we explore further the effect of patterning on the SERS EF of NPG using disk-shaped structures (NPGDs).[16] Our approach features hybrid fabrication by combining top-down planar large-area sputter etching and bottom-up atomic self assembly during dealloying. The resulted structure is thus hierarchical with the external disk shape and the internal porous network. We have selected 785 nm as the laser excitation wavelength and benzenethiol (BT) molecules as the SERS marker since the absence of a BT absorption peak near 785 nm minimizes the ambiguity presented by resonant Raman scattering, while the ability of BT to form self-assembled monolayers (SAMs) enables the number of molecules on individual NPG disks to be quantified. Additionally, the SERS activity at 785 nm laser excitation has critical significance for deep tissue penetration in any potential biomedical applications.

The initial film stack, consisting of a 75 nm thick Au : Ag = 28 : 72 alloy film over a 300 nm thick base layer of Au, was deposited by DC sputtering. The gold target was a 99.99% pure, Maple Leaf coin (Royal Canadian Mint); the alloy target was provided by ACI Alloys. The deposition rates for the gold and alloy films were 37.5 nm min^{-1} and 25 nm min^{-1}, respectively. The stack was patterned by RF-sputter-etching in 99.999% argon gas through a drop-coated mask of 500 nm polystyrene (PS) beads. RF-etching was timed to produce completely isolated alloy disks each sitting on a 65 nm thick solid gold pedestal; the remaining gold film provides a ground plane about 235 nm thick. The PS spheres were removed by sonication in isopropanol for 30 s. Ag was selectively dissolved by dipping

---

Department of Electrical and Computer Engineering, University of Houston, 4800 Calhoun Road, Houston, Texas 77204, USA. E-mail: wshih@uh.edu

† Electronic supplementary information (ESI) available: Detailed fabrication process, large area SERS mapping with corresponding SEM and optical micrographs, as well as discussion of the detection limit in terms of integration time and CCD temperature. See DOI: 10.1039/c2nr33242f

in 70% room temperature HNO_3 followed by deionized water rinse and nitrogen dry to form the NPGDs. The entire dipping-transfer procedure took ~5 s. The residual Ag content has been determined to be <10% by energy dispersive spectrometry (for details see ESI†).

Fig. 1a shows the nanoporous top surface of the NPGDs after removal of the PS beads and HNO_3 dissolution. The NPGDs are ringed by a gold film which is redeposited during sputter etching of the base layer after the alloy discs are defined. These rings are not affected by HNO_3 etch. The ultra-fine nanoporous network inside the disk is similar to that obtained in unpatterned NPG thin films (Fig. 1b) fabricated by the same dealloying procedure. The cracks caused by shrinkage during Ag dissolution are quite similar as well.[17]

Benzenethiol SAMs were deposited on unpatterned NPG, NPGD, and Klarite (SERS EF at least 10^6 for benzenethiol, Renishaw) substrates following the procedure of ref. 18. SERS measurements were carried out with 785 nm excitation using a home-built line-scan Raman microscopy system[19] enabling SERS mapping over $133 \times 133\ \mu m^2$ regions with $\sim 1\ \mu m^2$ resolution (full width at half maximum, FWHM) at a spectral resolution $\sim 8\ cm^{-1}$. Fig. 2 shows the SERS spectra in CCD count rate (CR), normalized to laser power and the area of the laser spot, for BT SAMs on NPGD, NPG, and Klarite substrates, as well as the normal Raman spectrum obtained from neat benzenethiol solution (the curves are offset for clarity). The CR for NPGD substrates is 517 times larger than for unpatterned NPG and 396 times larger than for Klarite. Since the nanoporous structure and thickness are identical for the NPGD and unpatterned NPG substrates, including the density and average size of the cracks, the patterning process has produced a 517-fold increase in enhancement factor. The interpretation of the increased Raman scattering of the NPGD *versus* Klarite substrate requires an estimate of the total number of BT molecules attached to a disk and how many of those are close enough to the surface to contribute to the measured photons.

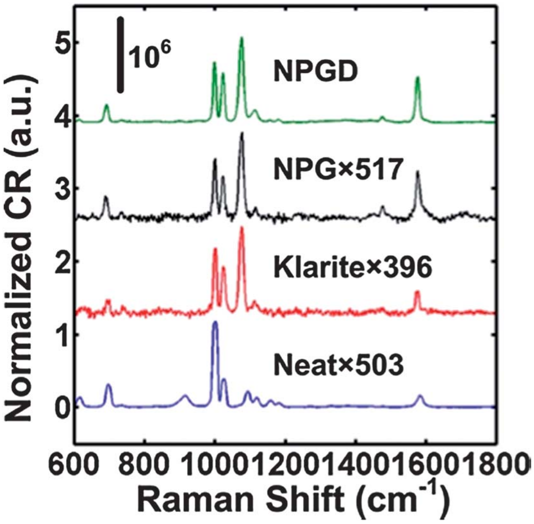

Fig. 2 Normalized count rate (CR) from NPGD, unpatterned NPG, Klarite, and neat benzenethiol *vs.* Raman shift (cm^{-1}).

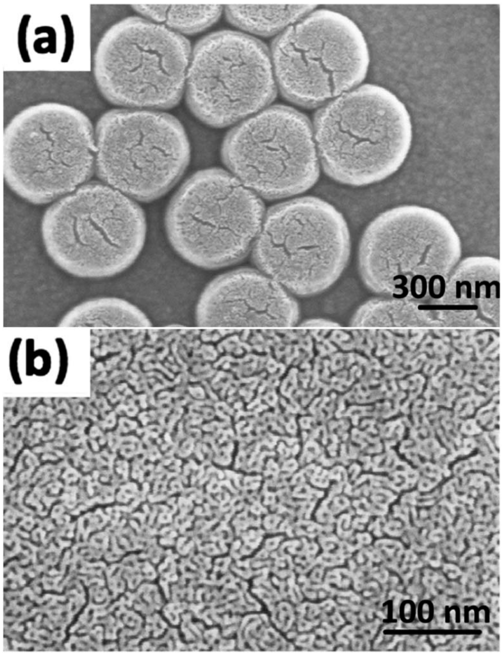

Fig. 1 (a) Top view of NPGDs ringed by gold; (b) unpatterned NPG film.

The number of adsorbed BT molecules in and on an NPG disk is the product of the area of the disk, the roughness R of NPG (the ratio of the chemically active surface area to the geometrical surface area), and the BT surface density. Ref. 20 describes a procedure for estimating the roughness of an NPG film from SEM images of the surface, assuming uniform nanostructure through the film. Equation 3 implies that roughness is given by $3h\beta/r$, where h, β, and r are the thickness, 2-dimensional porosity, and mean pore radius, respectively. An analysis of Fig. 1, using ImageJ (http://rsbweb.nih.gov/ij/), gives $\beta = 34\%$ and $r = 3.5$ nm, implying that the roughness is 22. Ref. 21 reports electrochemically measured roughness values in this range for 100 nm thick films with similar nanostructure. The roughness of Klarite is about 1.6 because of the increased surface area of the anisotropically etched pits.

The contribution of adsorbed molecules to the total SERS signals decreases with depth because of the decreasing laser power density and increased absorption of the Raman-scattered light. The contribution dR' of an NPG layer of thickness dt at depth h to Raman scattering is characterized by a roughness $dR' = R/h \times \exp(-2t/\alpha_{NPG}) \times dt$. Integration gives the effective roughness of the NPG taking into account the round-trip absorption; $R' = R \times \{\alpha_{NPG}/(2h) \times [1 - \exp(-2h/\alpha_{NPG})]\}$ where $\alpha_{NPG} = \alpha_{Au}/f_{Au}$ is the skin-depth of NPG, α_{NPG} is the skin depth of gold (~12.6 nm (ref. 22)), and f_{Au} is the mole fraction of Au in the Au/Ag alloy. We find that $R' = 6.3$ and $\alpha_{NPG} = 45$ nm. Following ref. 12, we have $EF_{NPGD}/EF_{Klarite} = \{CR_{NPGD}/R'_{NPGD}\}/\{CR_{Klarite}/$

Table 1 SERS EF estimation using Klarite at 785 nm excitation

	Klarite	NPGD	NPG film
EF of 1076 cm^{-1}	1×10^6	1.05×10^8	2.03×10^5
EF of 1575 cm^{-1}	1×10^6	1.43×10^8	2.47×10^5

Table 2 SERS EF estimation using neat solution sat 785 nm excitation[a]

	Probing depth (μm)	Probing volume (μm^3)	N_{neat} (molecules)	I_{neat} (photons s^{-1} mW^{-1})	EF
Method 1	4.5	1025.3	6.0×10^{12}	310.8	2.9×10^8
Method 2	3	585.1	3.4×10^{12}	97.7	5.2×10^8

[a] Method 1: experimentally characterized depth-of-focus; method 2: coverslip sandwich with 3 μm PS as spacers, the average depth estimated by benzenethiol solution volume divided by total spreading area.

$R_{Klarite}\}$, where the subscripts correspond to EF, CR, R, and R' of NPGD and Klarite. If the EF of Klarite is assumed as 1.0×10^6, although it is specified as *at least* according to the data sheet, the SERS enhancement factors calculated for 1076 cm^{-1} and 1575 cm^{-1} of NPGD substrates are 1.05×10^8 and 1.43×10^8 while those of unpatterned NPG film are 2.03×10^5 and 2.47×10^5, respectively (Table 1). We note that additional factors such as volumetric shrinkage may result in a slightly smaller R', and consequently a slightly larger EF, but it is not considered here because there is no obvious shrinkage in our SEM images before and after dealloying.

Alternatively, SERS enhancement factor can be obtained by comparing the SERS measurement to that from a neat benzenethiol sample, as outlined in ref. 23, where the EF value is calculated by comparing the 1575 cm^{-1} peak in the SERS spectrum to the 1584 cm^{-1} peak in neat Raman spectrum.[23] When the SERS and normal Raman spectra are measured by the same instrument, the SERS EF is given by EF = $\{I_{SERS}/I_{neat}\} \times \{N_{neat}/N_{SERS}\}$, where I_{SERS} and I_{neat} represent the normalized count rates of the SERS spectra from a single disk and normal Raman signal from a neat solution, respectively. N_{SERS} and N_{neat} are the number of molecules contributing to the SERS and neat Raman spectra, respectively. As discussed before, the "effective" surface area of NPGD is 6.3 times larger than its geometrical area. Assuming a packing density of 6.8×10^{18} molecules per m^2, approximately 8.4×10^6 molecules are adsorbed on a single disk. Therefore, the normalized count rate of the 1575 cm^{-1} peak from 5 NPG disks (which have a total area of ~1 μm^2) is 6.5×10^5 photons s^{-1} mW^{-1} (I_{SERS}; see Fig. 1), and is contributed by $5 \times 8.4 \times 10^6 = 4.2 \times 10^7$ molecules (N_{SERS}).

To obtain I_{neat} and N_{neat}, we performed two experiments with different ways to determine the optical probing depth. The optical probing volume was then calculated using the Gaussian beam with a 1.2 μm beam waist. In method 1, the depth of focus of our Raman instrument was experimentally characterized to be ~4.5 μm,[19] and then used as the probing depth. In method 2, a sparse monolayer of 3 μm polystyrene beads were sandwiched between two glass coverslips, squeezed and fixed. A drop of 2 μL neat benzenethiol was then dispensed and drawn into the gap between the 25 mm × 25 mm coverslips by capillary force. Based on the spreading area of the solution, the average thickness of benzenethiol was calculated to be ~3 μm. Table 2 lists the optical probing depth, probing volume, number of benzenethiol molecules (N_{neat}), normalized count rate of the 1584 cm^{-1} peak in the normal Raman spectra (I_{neat}, see Fig. 1), and enhancement factor (EF) from each method. The lowest EF value is slightly larger than the result obtained previously by assuming that Klarite has an enhancement factor of 1 million. We note again that Klarite is specified as *at least* 1 million.

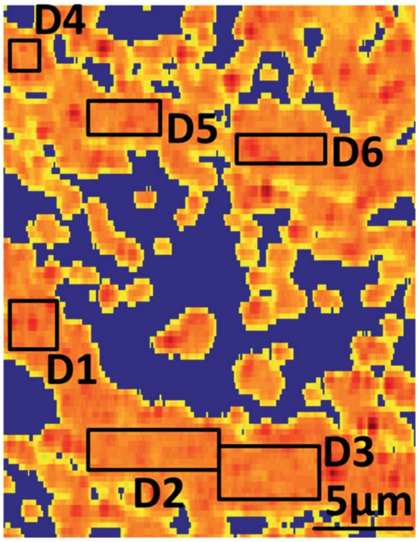

Fig. 3 SERS map of NPGDs obtained by the line-scan Raman system.

Since there is no modification to the nanoporous network from our patterning technique, the EF increase is entirely due to the disk formation. A heuristic explanation to the substantial EF increase is a red shift of the plasmonic resonance peak toward the laser excitation wavelength (785 nm) by patterning into submicron disk. This is supported by known red-shifted plasmonic resonance peak in solid gold disks.[14,15] Thus, it is plausible that plasmonic coupling between the external disk shape and the internal nanoporous network has contributed the high EF. Nevertheless, future work is needed to further unravel the

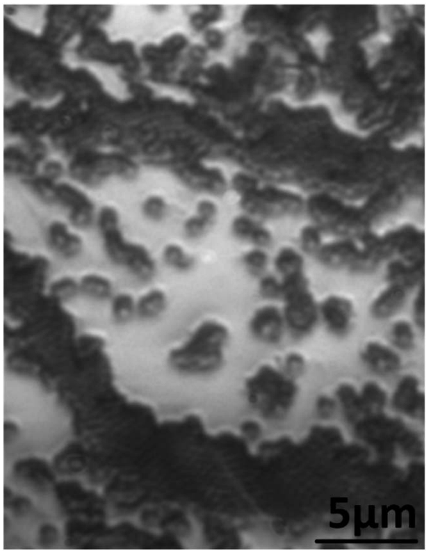

Fig. 4 Bright-field image of NPGDs from the same region as in Fig. 3.

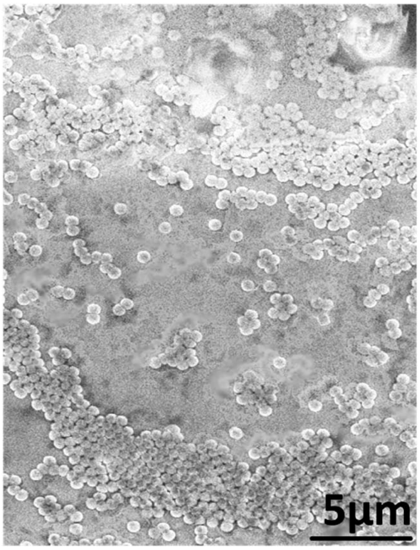

Fig. 5 SEM image of NPGDs from the same region as in Fig. 3.

interplay between the external shape and the internal network, as well as the identification of potential effects due to hot spot formation.

Fig. 3–5 show line-scan SERS, bright-field optical, and scanning electron microscope images of the same region on a NPGD sample, respectively. The SERS map was generated using the peak at ~1076 cm^{-1} (CCC stretch, CS bending) as shown in Fig. 2. Clearly, SERS signal is maximum on the disks. The disks appear larger in the SERS map due to the limited resolution of the line-scan Raman system. Thus, given the spatial resolution of ~1 μm, the pixel intensity of Fig. 3 is contributed by ~5 NPGDs for densely populated regions and from 1 NPGD for isolated disks. We have verified that the intensity is proportional to the number of disks. The SERS count rates from different locations marked by boxes in Fig. 3 are shown in Fig. 6. The standard deviation of the normalized count rate obtained from individual disks within 6 areas is ±32%, signifying a decent disk-to-disk uniformity. We note that the pattern uniformity can be much improved by nanosphere lithography[24] or electron-beam lithography, but is not the focus of this study. We have performed large-area SERS mapping on several other regions on the NPGD samples and obtained similar results as shown in Fig. S3 in ESI.†

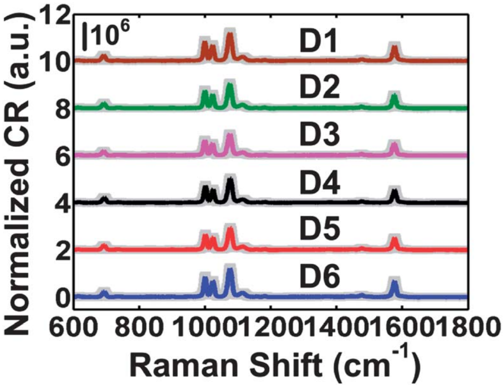

Fig. 6 Mean SERS spectra and ±1 standard deviation (in grey shade) of BT SAMs obtained from 6 areas marked in Fig. 3.

Given that the BT surface density on gold reported in the literature is 6.8×10^{14} cm^{-2}, the number of BT molecules on a single NPGD is ~14 attomoles. Since the signal-to-noise ratio (SNR) for NPGD is ~400 in Fig. 2, the detection limit is estimated to be ~22 100 BT molecules or 114 zeptomoles (SNR = 3) with 170 μW μm^{-2} laser power density and 2 s charge coupled device (CCD) integration time (Princeton BR400). We present more data on rapid detection with an uncooled CCD detector in ESI.†

In conclusion, we have shown that nanoporous gold disks are highly effective SERS substrates with an enhancement factor of ~10^8, about 517 times higher than for unpatterned NPG films. This is significantly higher than the value 10^3–10^4 that we estimate for the NPG disks discussed in ref. 13 by comparing to solid gold disks published in ref. 14 and 15. The detection limit of benzenethiol self-assembled monolayer on a single NPGD is estimated to be 114 zeptomoles at SNR = 3. Our studies suggest that NPGDs may provide the basis for SERS substrates with very high sensitivity, uniformity, and capacity for monolithic sensor chip technology.

WCS acknowledges funding from the National Science Foundation (NSF) CAREER Award (CBET-1151154), the National Aeronautics and Space Administration (NASA) Early Career Faculty Grant (NNX12AQ44G), the Gulf of Mexico Research Initiative (GoMRI-030) and the Cullen College of Engineering at the University of Houston. JCW acknowledges the partial support of the Texas Center for Superconductivity, the Alliance for Nanohealth, and the Cullen Foundation for a Lillie and Hugh Cranz Cullen Distinguished University Professorship. CB, JCW and WCS acknowledge NSF REU (EEC-1002509). We thank Szu-Te Lin for taking the SEM image shown in Fig. 5.

Notes and references

1 K. Kneipp, Y. Wang, H. Kneipp, L. T. Perelman, I. Itzkan, R. Dasari and M. S. Feld, *Phys. Rev. Lett.*, 1997, **78**, 1667–1670.
2 C. L. Haynes, A. D. McFarland and R. P. Van Duyne, *Anal. Chem.*, 2005, **77**, 338A–346A.
3 L. Malfatti, P. Falcaro, B. Marmiroli, H. Amenitsch, M. Piccinini, A. Falqui and P. Innocenzi, *Nanoscale*, 2011, **3**, 3760–3766.
4 J. P. Camden, J. A. Dieringer, J. Zhao and R. P. Van Duyne, *Acc. Chem. Res.*, 2008, **41**, 1653–1661.
5 A. Wittstock, V. Zielasek, J. Biener, C. M. Friend and M. Baumer, *Science*, 2010, **327**, 319–322.
6 S. O. Kucheyev, J. R. Hayes, J. Biener, T. Huser, C. E. Talley and A. V. Hamza, *Appl. Phys. Lett.*, 2006, **89**, 053102.
7 D. Gloria, J. J. Gooding, G. Moran and D. B. Hibbert, *J. Electroanal. Chem.*, 2011, **656**, 114–119.
8 Y. Yang, Y. Xia, W. Huang, J. Zheng and Z. Li, *J. Solid State Electrochem.*, 2012, **16**, 1733–1739.
9 J. Biener, G. W. Nyce, A. M. Hodge, M. M. Biener, A. V. Hamza and S. A. Maier, *Adv. Mater.*, 2008, **20**, 1211–1217.

10 X. Lang, L. Qian, P. Guan, J. Zi and M. Chen, *Appl. Phys. Lett.*, 2011, **98**, 093701.

11 L. Zhang, X. Lang, A. Hirata and M. Chen, *ACS Nano*, 2011, **5**, 4407–4413.

12 Y. Jiao, D. Ryckman, P. N. Ciesielski, C. A. Escobar, G. K. Jennings and S. M. Weiss, *Nanotechnology*, 2011, **22**, 295302.

13 J.-S. Wi, S. Tominaka, K. Uosaki and T. Nagao, *Phys. Chem. Chem. Phys.*, 2012, **14**, 9131–9136.

14 S. W. Lee, K. S. Lee, J. Ahn, J. J. Lee, M. G. Kim and Y. B. Shin, *ACS Nano*, 2011, **5**, 897–904.

15 Q. Yu, P. Guan, D. Qin, G. Golden and P. M. Wallace, *Nano Lett.*, 2008, **8**, 1923–1928.

16 W.-C. Shih, *US Pat.* Application 61/609, 451, 2012.

17 D. Kramer, R. N. Viswanath and J. Weissmuller, *Nano Lett.*, 2004, **4**, 793–796.

18 M. E. Abdelsalam, P. N. Bartlett, J. J. Baumberg, S. Cintra, T. A. Kelf and A. E. Russel, *Electrochem. Commun.*, 2005, **7**, 740–744.

19 J. Qi, P. Motwani, J. C. Wolfe and W.-C. Shih, *Proceedings of SPIE*, San Francisco, 2012.

20 E. Seker, Y. Berdichevsky, M. R. Begley, M. L. Reed, K. J. Staley and M. L. Yarmush, *Nanotechnology*, 2010, **21**, 125504.

21 M. D. Scanlon, U. Salaj-Kosla, S. Belochapkine, D. MacAodha, D. Leech, Y. Ding and E. Magner, *Langmuir*, 2012, **28**, 2251–2261.

22 P. B. Johnson and R. W. Christy, *Phys. Rev. B: Condens. Matter Mater. Phys.*, 1972, **6**, 4370–4379.

23 R. L. Aggarwal, L. W. Farrar, E. D. Diebold and D. L. Polla, *J. Raman Spectrosc.*, 2009, **40**, 1331–1333.

24 C. L. Haynes and R. P. Van Duyne, *J. Phys. Chem. B*, 2001, **105**, 5599–5611.